The role of bacteriotherapy timing in microbiome recovery

Eric W. Jones* and Jean M. Carlson
Department of Physics, University of California, Santa Barbara, California 93106, USA
(Dated: August 7, 2018)

In the gut microbiome, the successful administration of fecal microbiota transplantation (FMT) will convert a diseased microbial composition into a healthy one. We idealize the microbiome as a two-state ecological system and investigate the efficacy of FMT, a type of bacteriotherapy, on fragile antibiotic-disrupted microbial states. We observe that FMT is most effective when administered immediately or nearly immediately after antibiotics, and that a delay in FMT administration may undermine its success. We find that the role of FMT timing is tied to the fast and slow manifolds of a semistable fixed point. From this, we explicitly derive how the required FMT transplant size depends on the timing of its administration. Finally, we introduce *steady state reduction*, an ecologically-inspired model reduction technique that draws a correspondence between this two-state model and an experimentally derived model of antibiotic-induced *C. difficile* infection.

Since the realization that the microbiome profoundly influences host health, diseases ranging from inflammatory bowel disease to cancer have been found to be associated with aberrant microbial compositions in the gut, a diseased state known as *dysbiosis* [1]. A promising frontier of medicine relies on the notion that the composition of the microbiome can both influence and be influenced by disease, so that the deliberate alteration of the microbiome via *bacteriotherapy* may be a viable treatment option for a range of diseases [2, 3]. Perhaps the clearest evidence for this is the success that fecal microbiota transplantation (FMT), a type of bacteriotherapy in which gut microbes from a healthy donor are engrafted in an infected patient, has had in treating recurrent *C. difficile* infection (CDI) [4].

Historically, FMT-like therapies have been used to treat gastrointestinal distress since 4th century China under the guise of "yellow soup" [5]. Today, FMT is an emerging alternative to antibiotics [6, 7], in part because FMT does not contribute to antimicrobial resistance. Therefore, ecological frameworks are being actively developed that describe how bacteriotherapies can regulate the microbiome [8–10], and experimental studies are leveraging these frameworks to design and test "optimal" FMT therapies [11].

Thousands of microbial species populate the gut microbiome [14], but for modeling purposes it is common to coarse-grain at the genus or phylum level. For example, Stein et al. [9] fit an 11-dimensional genus-level ecological model of CDI with bacterial abundance data from a mouse experiment [15]. Despite the fact that this model did not resolve individual species, it still captured the clinically- and experimentally-observed phenomenon of antibiotic-induced CDI, suggesting that the true microbiome's dimensionality could be approximated by an 11-dimensional model.

In this letter we simplify the dimensionality of the microbiome even further: instead of thousands of microbial species or eleven dominant genera, we consider each steady state of the microbiome as a single idealized ecological population. By considering two such steady states (construed as healthy and diseased), we analyze a two-state ecological system that demonstrates how FMT and antibiotic administration can induce a lasting shift in microbial composition.

We take advantage of the analytic tractability of this two-state model to investigate the role of FMT timing on its efficacy. While manipulating a treatment's time course has innovated treatment strategies in cancer im-

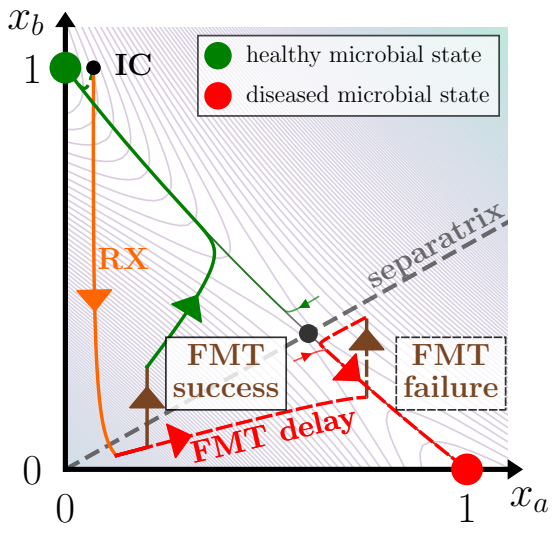

FIG. 1. The success or failure of fecal microbiota transplantation (FMT) depends on the timing of its administration. We consider the two-state ecological system of Eq. (1) in a clinically-inspired scenario. First, a health-prone initial condition (IC) is depleted by antibiotics (RX, orange). If FMT (brown) is administered shortly after the antibiotics, the treatment steers the composition to a healthy state (FMT success). If FMT administration is delayed, the microbial trajectory instead attains the diseased state (FMT failure). The basins of attraction of the healthy and diseased steady states are delineated by the separatrix, and isoclines of the system's potential energy landscape (light contours) are given by the split Lyapunov function Eq. (S21) [17].

munotherapy [12] and HIV vaccination [13], this perspective has not been previously considered in the context of bacteriotherapy. We discover the clinically-relevant prediction that delaying the administration of FMT can lead to its failure, as in Fig. 1.

To this end, we focus on a scenario in which antibiotics deplete a health-prone initial condition, requiring administration of FMT in order to recover (illustrated in Fig. 1). Since this scenario parallels antibiotic-induced CDI, later in the letter we find a parameter mapping that reduces the genus-level CDI model [9] to an effective two-state system that mimics the genus-level dynamics. We call this model reduction technique *steady state reduction*, and argue that the correspondence between the two systems is evidence of a generic capacity for dimensionality reduction in ecological systems.

We consider the generalized Lotka-Volterra equations in two-dimensions [16]. Here, the trajectories of two populations x_a and x_b are given by

$$\begin{aligned}\frac{\mathrm{d}x_a}{\mathrm{d}t} &= x_a(\mu_a - M_{aa}x_a - M_{ab}x_b) \\ &\quad + x_a\varepsilon_a u(t) + w_a\delta(t-t^*) \quad \text{and} \\ \frac{\mathrm{d}x_b}{\mathrm{d}t} &= x_b(\mu_b - M_{ba}x_a - M_{bb}x_b) \\ &\quad + x_b\varepsilon_b u(t) + w_b\delta(t-t^*),\end{aligned} \tag{1}$$

with growth rates $\vec{\mu}$ and interactions M, optional antibiotic administration $u(t)$ operating with efficacy $\vec{\varepsilon}$, and optional FMT with transplant $\vec{w}$ at time t^*. The two-dimensional state vector $\vec{x} = (x_a,\ x_b)$ is composed of components x_a and x_b that (in our abstraction) are the magnitudes of the contributions from the *diseased* and *healthy* steady states, respectively. Though the transplant $\vec{w}$ can consist of a mixture of the healthy and diseased steady states, in this letter we assume that the transplant consists of exclusively healthy microbes so that $w_a = 0$.

Through nondimensionalization we set $M_{aa} = M_{bb} = \mu_a = 1$, and to simplify the presentation of our results we assume $\mu_b = 1$. In the Supplementary Information [17] we verify that the results of this letter hold for $\mu_b \neq 1$, and provide the explicit calculations supporting this letter's claims. The figures in this letter are generated with the randomly chosen yet representative parameter values $M_{ab} = 1.167$ and $M_{ba} = 1.093$.

The dynamical system Eq. (1) exhibits three nontrivial steady states at $(1,\ 0)$, $(0,\ 1)$, and $(x_a^*,\ x_b^*)$, where $0 < x_a^* < 1$ and $0 < x_b^* < 1$ with their precise forms given in Eq. (S4) [17]. Since we are interested the switching behavior between healthy and diseased states, we only consider systems in which the two homogeneous steady states are stable, which forces the mixed steady state $(x_a^*,\ x_b^*)$ to be semistable [17].

The long-term dynamics of this system are dictated by the basins of attraction of the stable steady states,

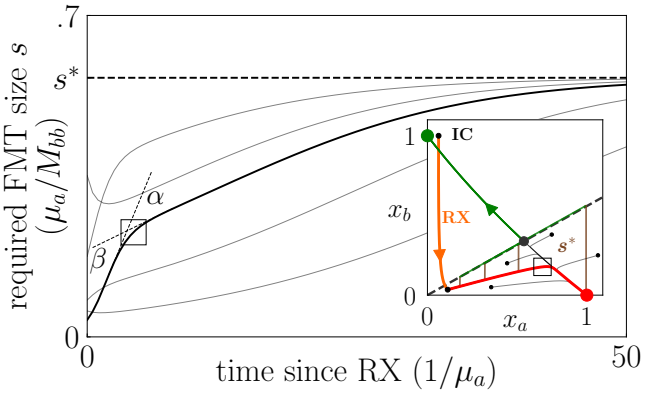

FIG. 2. The FMT transplant size needed to revert an antibiotic-depleted state back to health grows as FMT administration is delayed. We calculate the minimum FMT transplant size required to cure five disease-prone microbial trajectories that evolve according to Eq. (1). As trajectories attain the diseased steady state, the required transplant size approaches s^*. The required transplant size changes at two different rates, α and β, with the crossover point between these two rates indicated by a hollow square. The transplant size dynamics $\mathrm{d}s/\mathrm{d}t$ as well as the rates α and β are derived in Eq. (3) and the surrounding text.

and these basins are delineated by a separatrix that, for topological reasons, must be the stable manifold of the semistable fixed point $(x_a^*,\ x_b^*)$. In Fig. 1 these basins are represented topographically as isoclines of the split Lyapunov function $V(x_a, x_b)$ (lightly shaded contours), which acts as a potential energy landscape [17, 18].

We analytically compute this stable manifold in a power series expansion about the semistable fixed point as a function of the gLV system parameters in Eq. (S20) [17], which enables us to classify the fate of a given initial condition *a priori*. Therefore, altering the fate of an initial condition requires crossing the separatrix with some external intervention, for example by FMT.

At each point along a microbial trajectory in the diseased basin of attraction, we may calculate the minimum FMT size s required to transfer the microbial state into the healthy basin of attraction. We use this metric to quantify our notions of "FMT efficacy." In Fig. 2 we present s as a function of time (main panel) for several trajectories that originate in the diseased basin of attraction (inset), including the main trajectory of Fig. 1. We find that the minimum FMT size increases with time—often dramatically— and that there are two discernible rates of increase, which we denote α and β in the figure. In the following text, we link these two rates to the fast and slow manifolds of the ecological system, and we derive an expression that governs the minimum required transplant size over time.

To reflect the importance of the separatrix in dictating the microbial dynamics, we change coordinates to the eigenvectors $(u,\ v)$ of the semistable steady state, shown

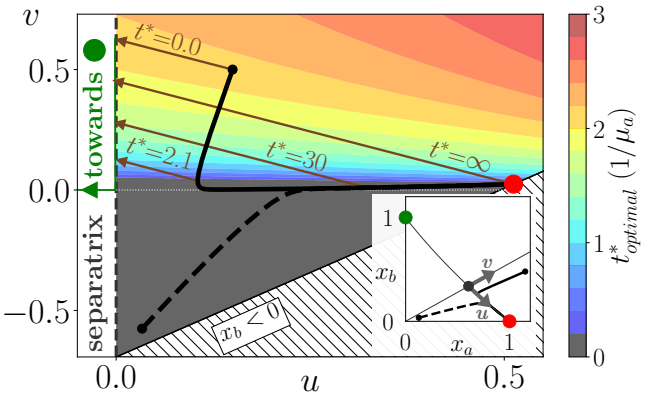

FIG. 3. The role of timing in FMT administration. For disease-prone initial conditions, FMT is most effective when administered immediately ($t^*_{opt} = 0$, grey) or nearly immediately ($t^*_{opt} > 0$, colored). We can calculate the optimal transplant time t^*_{opt} for any initial condition (u_0, v_0) (colorbar) according to Eq. (S62) of [17], which can reduce to Eq. (4). We show two microbial trajectories that are plotted in (u, v) (main panel) and (x_a, x_b) (inset) coordinates. For $v_0 > 0$ we show four possible FMT transplants, including the optimal one that occurs at $t^*_{opt} = 2.1$. For $v_0 < 0$ it is always best to administer FMT immediately.

in Fig. 3 (inset). In these coordinates the v-axis corresponds to the separatrix, and u is proportional to the minimum FMT size required for a successful transplant s, such that $s = u/(\hat{u} \cdot \hat{x}_b)$, where ($\hat{u}$, $\hat{v}$) and ($\hat{x}_a$, $\hat{x}_b$) are the unit vectors associated with their associated coordinates.

In this new (u, v) basis, the gLV equations (1) become

$$\begin{aligned} \frac{\mathrm{d}u}{\mathrm{d}t} &= A_{10}u - A_{11}uv - A_{20}u^2 \\ \frac{\mathrm{d}v}{\mathrm{d}t} &= -B_{01}v - B_{02}v^2 + B_{20}u^2, \end{aligned} \tag{2}$$

where each coefficient is a positive algebraic function of the original gLV parameters that we have analytically determined in Eqs. (S36-S48) [17]. When $\mu_b \neq 1$, these equations contain additional quadratic terms described in [17]. Naturally, in the small u and small v limit this model reduces to the linearization about the semistable fixed point. Near this fixed point there is a separation of time scales between u and v ($B_{01}/A_{10} > 1$, with median of 5.9 and IQR of [2.7, 9.1] over random parameter draws [17]), indicating that there are inherent fast and slow manifolds in this system.

This coordinate change also reveals the role of timing in FMT administration, since the minimum required transplant size s is precisely governed by Eq. (2), by proxy of u. To demonstrate this analytically, we consider an initial condition condition (u_0, v_0) that is located near the fast manifold in a system with clear separation of time scales, so that (i) $B_{20}u_0^2$ is small, (ii) $B_{01} >> A_{10}$, and (iii) $B_{02}v_0^2 << B_{01}v_0$ (though we relax this assumption in Eq. (S62) [17]). In this case, the dynamics in the fast $\hat{v}$ direction may be approximated as $v(t) \approx v_0 \mathrm{e}^{-B_{01}t}$, and so the required transplant size dynamics become

$$\frac{\mathrm{d}s}{\mathrm{d}t} = s\left(A_{10} - A_{20}(\hat{u} \cdot \hat{x}_b)s - A_{11}v_0\mathrm{e}^{-B_{01}t}\right). \tag{3}$$

With Eq. (3) we can interpret the rates of increase in required transplant size s of the main trajectory in Fig. 2, α and β [17]. Specifically, $\alpha = \frac{\mathrm{d}s(0)}{\mathrm{d}t}\big|_{s=s_c}$ and $\beta = \frac{\mathrm{d}s(\infty)}{\mathrm{d}t}\big|_{s=s_c}$ where s_c is the transplant size required at the crossover point between these rates.

For an initial condition with $v_0 < 0$, which can occur when a nearly healthy state is depleted by antibiotics as in Fig. 1, we have $\alpha > \beta$. In this case the required transplant size monotonically increases until it attains s^* at the infected steady state, and so it is best to administer FMT as soon as possible. Alternatively, when $v_0 > 0$ we have $\alpha < \beta$. When $A_{11}v_0$ is sufficiently large α can become negative, which means that there is a nonzero transplant time at which the required transplant size is minimized (corresponding to $\frac{\mathrm{d}s}{\mathrm{d}t} = 0$). The concave-up trajectories in Fig. 2 exhibit this optimal transplant time. For $v_0 > 0$ and under the same conditions for which Eq. (3) was derived, we find that this optimal transplant time t^* is

$$t^*_{opt} = \frac{1}{B_{01}} \ln\left(\frac{A_{11}v_0}{A_{10} - A_{20}u_0}\right). \tag{4}$$

This nonzero transplant time reflects ecological pressures that temporarily drive the system closer to the separatrix, overpowering the slow unstable manifold. In Fig. 3 we show two trajectories that numerically recapitulate these two cases.

Therefore, these results describe the influence of timing on FMT administration and specify that there is an optimal time (either immediately or at t^*_{opt}) at which to drive conversion between steady states in two-state systems.

To further broaden this result we now demonstrate that high-dimensional gLV systems can be projected into the two-state form of Eq. (1). We consider the previously mentioned 11-dimensional model of CDI in mice constructed by Stein et al. [9]. We show that the basins of attraction qualitatively agree in the 11-dimensional (11D) and two-dimensional (2D) forms. In addition, we demonstrate that the timing phenomena we identified in 2D— that it is better to apply FMT sooner than later, and that the required transplant size dynamics $\frac{\mathrm{d}s}{\mathrm{d}t}$ vary along slow and fast manifolds— are preserved in 11D. Therefore, we argue that we can employ our 2D results to build intuition and evaluate the efficacy of FMT in the 11D system.

The CDI model takes the same form as Eq. (1) but tracks the abundances of 10 different microbial genera and the pathogen *C. difficile* (CD), all of which can inhabit the mouse gut. For each microbial population y_i,

the model reads

$$\frac{\mathrm{d}}{\mathrm{d}t}y_i(t) = y_i(t)\left(\rho_i + \sum_{j=1}^{11} K_{ij}y_j(t) + \zeta_i u(t)\right). \quad (5)$$

The parameters of this model, analogous to those of Eq. (1), were fit with data from an experimental mouse study [15]. In real life, antibiotic administration can deplete the microbiome and prompt CDI, and this phenomenon is captured by the model as well. In previous work studying this model [10] we created phase diagrams that demonstrated how antibiotic administration induced vulnerability to CDI, and showed that FMT could successfully salvage a CDI-prone microbial state. Notably, these properties are exhibited in our 2D system as well.

We now demonstrate that we can simplify the high-dimensional system to 2D while retaining this switching behavior through *steady state reduction* (SSR). We focus on two steady states of the high-dimensional model: a CD-susceptible (diseased) state $\vec{y}_a$, and a CD-resilient (healthy) state $\vec{y}_b$, with details given in [17].

In order to cast these steady states as the coordinates x_a and x_b of Eq. (1), we need to compress the high-dimensional parameters of Eq. (5) ($\vec{\rho}$, K, and $\vec{\zeta}$) into *effective* 2D parameters ($\vec{\mu}$, M, and $\vec{\varepsilon}$). To accomplish this we take $\mu_\gamma = \vec{\rho}\cdot\vec{y}_\gamma$ and $\varepsilon_\gamma = \vec{\zeta}\cdot\vec{y}_\gamma$ for $\gamma \in a,\ b$, and take $M_{\gamma\delta} = \vec{y}_\gamma^T K \vec{y}_\delta$ for $\gamma,\ \delta \in a,\ b$. Through this construction, the 2D system will exhibit steady states at (1, 0) and (0, 1) [17]. Further, when the high-dimensional steady states are stable, the corresponding 2D steady states will be stable as well [17], which guarantees the existence of a separatrix in the reduced 2D system.

Since the coarse-grained 11D model approximates features of the actual microbiome (consisting of thousands of species), testing how well SSR reduces the 11D model to 2D is therefore a proxy for how well SSR compresses the true high-dimensional microbiome into a 2D model with healthy and diseased steady states.

To compare the 11D and 2D models, in Fig. 4 we consider initial conditions located on the 2D plane embedded in 11D that is defined by the origin, $\vec{y}_a$, and $\vec{y}_b$, and note that we can project any point on this embedded plane to the 2D phase space of Eq. (1) [17]. Since the 11D system has been compressed, naturally the low- (lighter, solid) and projected high-dimensional (darker, dashed) trajectories do not exactly match. Still, there is a qualitative agreement between the two cases, especially in terms of the steady state attained by a given initial condition. To quantify this agreement, in Fig. 4 we contrast the basins of attraction for the 2D (large squares) and 11D (small squares) systems by tracking the fate of associated pairs of initial conditions in 2D and on the 2D plane embedded in 11D.

The time courses of the required transplant size s also qualitatively agree in both systems. The 11D microbial trajectory initially follows a fast stable manifold but

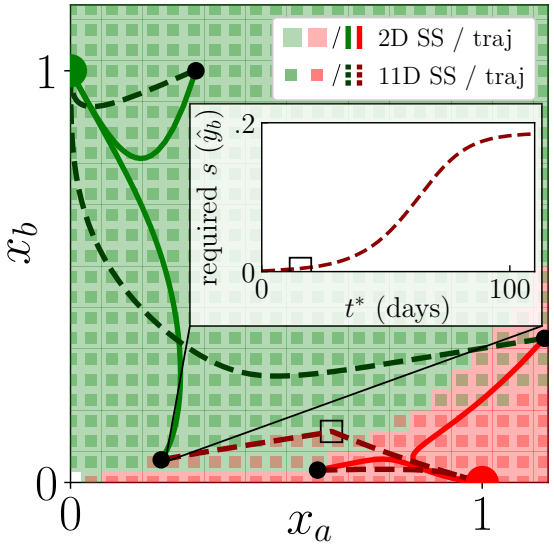

FIG. 4. An experimentally derived 11D gLV system Eq. (5) is compressed into a 2D counterpart Eq. (1) through steady state reduction (SSR). Healthy (green circle) and infected (red circle) steady states of the 11D system become basis vectors of the 2D system. We plot trajectories in the high- (darker dashed) and low-dimensional (lighter solid) systems, with the 11D trajectories projected onto a 2D plane. We generate basins of attraction for both systems by coloring initial conditions according to their fates in the high-dimensional (small squares, darker) and low-dimensional (large squares, lighter) simulations. (inset) As in 2D, in 11D the required transplant size s grows with administration delay. (color online)

then switches to the slow manifold of a high dimensional fixed point. As in the low-dimensional case, the flow along these fast and slow manifolds underpins the required transplant size s dynamics, where the transplant consists of healthy microbes $\vec{y}_b$. In the case of Fig. 4, the transition point between these two manifolds occurs at 15.6 days, and is indicated by a hollow square (main panel and inset). This high-dimensional case corroborates our previous timing results, and indicates that our findings may be a generic feature of ecological models.

Together, these findings— that the 2D model qualitatively captures the basins of attraction of the 11D model, and that features of the 2D model are also expressed in 11D— demonstrate that SSR can act as a conduit between tractable low-dimensional analysis and the realistic behavior of high-dimensional systems. In addition to the computational efficiency of this technique, which employs the earlier analytic results rather than expensive simulations, SSR generates an intuition for the high-dimensional system through 2D cross-sections that link different steady states. Further, SSR realizes a natural progression towards the simplification of dynamical systems: while linearization approximates a dynamical system about a single steady state, SSR approximates a dynamical system about *two* steady states.

While other model reduction techniques exist [20, 21], SSR differs by preserving core observable ecological features. For example, SSR could be directly applied to raw microbial data [22] and by construction choose basis vectors that correspond to experimentally observed steady states. The resulting models would consist of fewer yet more physically relevant variables and parameters, leading to improved explanatory power. More generally, this approach could be applied to data from any system where healthy and diseased states compete.

In this letter, we uncovered the ecological prediction that FMT would be more effective when administered soon after antibiotics in a classic ecological model. Additionally, this experimentally tractable hypothesis would test whether slow manifolds are present in real ecological systems, as well as inform the theory that underpins controlled navigation through high-dimensional microbial space. By anchoring high-dimensional systems to well-characterized two-dimensional ones, our techniques can help unravel the complicated landscape that accompanies complex systems and their behaviors.

This material was based upon work supported by the National Science Foundation Graduate Research Fellowship Program under Grant No. 1650114. Any opinions, findings, and conclusions or recommendations expressed in this material are those of the author(s) and do not necessarily reflect the views of the National Science Foundation. This work was also supported by the David and Lucile Packard Foundation and the Institute for Collaborative Biotechnologies through contract no. W911NF-09-D-0001 from the U.S. Army Research Office. The funders had no role in study design, data collection and analysis, decision to publish, or preparation of the manuscript.

* ewj@physics.ucsb.edu

[1] J. Lloyd-Price, G. Abu-Ali, and C. Huttenhower, Genome Medicine **8**, 51 (2016).
[2] V. B. Young, BMJ **356** (2017).
[3] J. E. Belizário and M. Napolitano, Frontiers in Microbiology **6**, 1050 (2015).
[4] D. Merenstein, N. El-Nachef, and S. V. Lynch, Journal of Pediatric Gastroenterology and Nutrition **59** (2014).
[5] P. F. de Groot, M. N. Frissen, N. C. de Clercq, and M. Nieuwdorp, Gut Microbes **8**, 253 (2017).
[6] T. J. Borody and A. Khoruts, Nature Reviews Gastroenterology & Hepatology **9**, 88 EP (2011).
[7] R. D. Heath, C. Cockerell, R. Mankoo, J. A. Ibdah, and V. Tahan, North Clin Istanb **5**, 79 (2018).
[8] J. Walter, M. X. Maldonado-Gómez, and I. Martínez, Current Opinion in Biotechnology **49**, 129 (2018).
[9] R. R. Stein, V. Bucci, N. C. Toussaint, C. G. Buffie, G. Rätsch, E. G. Pamer, C. Sander, and J. B. Xavier, PLoS Comput Biol **9**, 1 (2013).
[10] E. W. Jones and J. M. Carlson, PLOS Computational Biology **14**, 1 (2018).
[11] C. G. Buffie, V. Bucci, R. R. Stein, P. T. McKenney, L. Ling, A. Gobourne, D. No, H. Liu, M. Kinnebrew, A. Viale, E. Littmann, M. R. M. van den Brink, R. R. Jenq, Y. Taur, C. Sander, J. Cross, N. C. Toussaint, J. B. Xavier, and E. G. Pamer, Nature **517**, 205 (2015).
[12] D. J. Messenheimer, S. M. Jensen, M. E. Afentoulis, K. W. Wegmann, Z. Feng, D. J. Friedman, M. J. Gough, W. J. Urba, and B. A. Fox, Clinical Cancer Research **23**, 6165 (2017).
[13] S. Wang, PLOS Computational Biology **13**, 1 (2017).
[14] J. L. Round and S. K. Mazmanian, Nat Rev Immunol **9**, 313 (2009).
[15] C. G. Buffie, I. Jarchum, M. Equinda, L. Lipuma, A. Gobourne, A. Viale, C. Ubeda, J. Xavier, and E. G. Pamer, Infect Immun **80**, 62 (2012).
[16] J. Parrish and S. Saila, Journal of Theoretical Biology **27**, 207 (1970).
[17] Supplementary Information available at ****.
[18] Z. Hou, B. Lisena, M. Pireddu, F. Zanolin, S. Ahmad, and I. Stamova, *Lotka-Volterra and Related Systems: Recent Developments in Population Dynamics*, De Gruyter Series in Mathematics and Life Sciences (De Gruyter, 2013).
[19] Y. Tang, R. Yuan, and Y. Ma, Phys. Rev. E **87**, 012708 (2013).
[20] C. Gu, *Model order reduction of nonlinear dynamical systems*, Ph.D. thesis, UC Berkeley (2011).
[21] A. Goeke, S. Walcher, and E. Zerz, Physica D: Nonlinear Phenomena **345**, 11 (2017).
[22] P. I. Costea, F. Hildebrand, M. Arumugam, F. Bäckhed, M. J. Blaser, F. D. Bushman, W. M. de Vos, S. Ehrlich, C. M. Fraser, M. Hattori, C. Huttenhower, I. B. Jeffery, D. Knights, J. D. Lewis, R. E. Ley, H. Ochman, P. W. O'Toole, C. Quince, D. A. Relman, F. Shanahan, S. Sunagawa, J. Wang, G. M. Weinstock, G. D. Wu, G. Zeller, L. Zhao, J. Raes, R. Knight, and P. Bork, Nature Microbiology **3**, 8 (2018).